

HIGH TEMPERATURE FABRY-PEROT BASED STRAIN SENSOR
FOR CERAMIC CROSS FLOW FILTERS

K.A. Murphy, C.E. Koob, A.J. Plante,
M.F. Gunther, A.M. Vengsarkar and R.O. Claus

Fiber & Electro-Optics Research Center
Bradley Department of Electrical Engineering
Virginia Tech, Blacksburg, VA 24061 - 0111

INTRODUCTION

The objectives of this research program were to develop instrumentation methods to allow in-situ analysis of ceramic cross flow (CXF) filters. Information from such instrumentation is needed to determine how the filters perform during operation, how subsequent filter and combustor designs may be improved based on the knowledge of such performance, and how and where damage and degradation occur. CXF filters are used for hot gas clean-up of coal-fired power generation systems, such as pressurized fluidized-bed combustors and integrated gasifier-combined cycles. The ceramic cross flow filter is analogous to cross-flow heat exchangers, except gas is passed between channels instead of thermal energy (heat). The CXF filters are made from multiple layers of thin, flat, porous ceramic (alumina or silicon nitride) with grooves which form channels in each layer. The layers are stacked to form a filter element that is approximately 30 cm high by 30 cm long by 10 cm wide. Consecutive layers of ceramic are oriented such that the channels formed are perpendicular to each other. One of the sides of the filter element is sealed. Gas enters the filter through the openings of the channel on the two sides that are perpendicular to the sealed end, permeates the porous ceramic, and exits through the openings on the side that is parallel to the sealed end. Particles are removed from the gas stream by direct interception, diffusion, and inertial impaction. The filter elements are periodically backflushed with a brief, high-pressure cleaning pulse of air or nitrogen to remove the particles that were deposited on the dirty side of the dividing walls. The CXF filter operates in an extremely corrosive and erosive environment while undergoing temperatures between 500 and 900° C and pressures up to 2500 kPa.

Optical fiber sensors are ideally suited for the in-situ analysis of the CXF filter with operating temperatures up to 1000° C, electromagnetic disturbance immunity and small size. We present an optical fiber extrinsic Fabry-Perot interferometric strain sensor. The background of the sensor and a detailed description will be discussed first, followed by results from on-site testing of the fiber sensors at Westinghouse Science and Technology Center in Pittsburgh, PA.

SENSOR BACKGROUND AND DESCRIPTION

Fiber optic Fabry-Perot (FP) sensors reported in the literature have been highly sensitive to temperature, mechanical vibration, acoustic waves, and magnetic fields [1]. Techniques to create the FP cavity have varied from the creation of Bragg gratings in or on the fiber [2] to the use of air-glass interfaces at the fiber ends as the reflectors [3]. A relatively new technique described by Lee and Taylor involves fabricating semireflective splices in a continuous length of fiber [4]. In this Letter, we present an optical fiber extrinsic FP interferometer for measuring strain and microdisplacements.

Most FP sensors described in the past have been useful in the measurement of quasi-static strain alone. That is, when the induced strain changes its polarity, the FP interferometers would not be able to detect this change if the switch in direction took place at a maximum or minimum of the transfer function curve. Methods for obtaining directional strain information using thin-film, or resistive gauges have been demonstrated [5]. In a paper on two-mode elliptical-core fiber sensors, we have shown that the availability of two signals 90° shifted in phase will be able to resolve this issue [6]. In this Letter, we show that a technique based on the same principle can be used with extrinsic FP strain sensors to measure the relative direction of dynamically varying strain. A theoretical description of the sensor operation is presented and two different configurations to obtain a quadrature phase-shifted operation are described.

We first describe the construction of the extrinsic FP interferometer with reference to Figure 1. A single mode fiber ($\lambda_0 = 1300$ nm), used as the input/output fiber, and a multimode fiber, used purely as a reflector, form an air gap that acts as a low-finesse FP cavity. The far end of the multimode fiber is shattered so the reflections from the far end do not add to the detector noise. The Fresnel reflection from the glass/air interface at the front of the air gap (reference reflection) and the reflection from the air/glass interface at the far end of the air gap (sensing reflection)

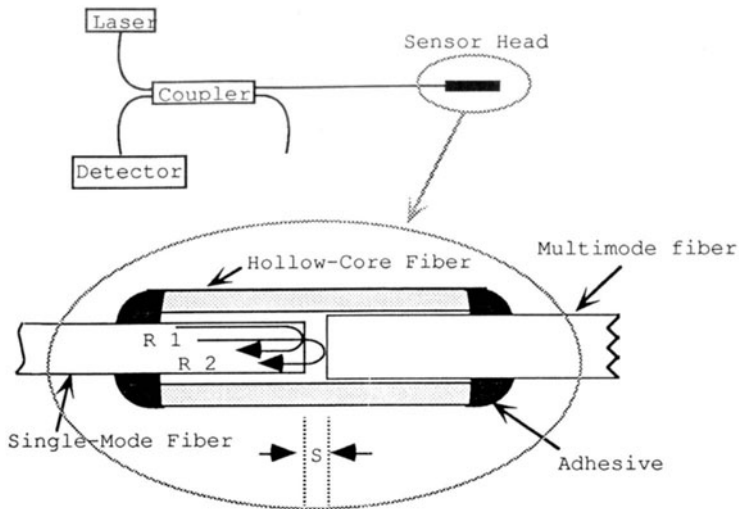


Fig. 1. Fabry-Perot sensor system with detail of sensor.

interfere in the input/output fiber. Although multiple reflections occur within the air gap, the effect of reflections subsequent to the ones mentioned above can be shown to be negligible. The two fibers are allowed to move in the silica tube and changes in the air gap length cause changes in the phase difference between the reference reflection and the sensing reflection. The phase difference can be monitored as intensity modulations at the output of a fused biconical tapered coupler.

We will evaluate the interference of the two-wave interferometer in terms of a plane-wave approximation. A coherent, approximately-plane wave detected at the output of the sensor can be represented in terms of its complex amplitude $U_i(x, z, t)$, given by

$$U_i(x, z, t) = A_i \exp(j\phi_i), \quad i = 1, 2, \quad (1)$$

where the variable A_i can be a function of the transverse coordinate x and the distance traveled, z , and the subscripts $i = 1, 2$ stand for the reference and the sensing reflections, respectively. Assuming that the reference reflection coefficient $A_1 = A$, the sensing reflection coefficient A_2 can be approximated by the simplified relation [7]

$$A_2 = A \left[\frac{ta}{a + 2s \tan(\sin^{-1}(NA))} \right], \quad (2)$$

where a is the fiber core radius, t is the transmission coefficient of the air-glass interface (≈ 0.98), s is the end separation and NA is the numerical aperture of the single-mode fiber, given by $NA = (n_1^2 - n_2^2)^{1/2}$. The terms n_1 and n_2

are the refractive indices of the core and the cladding, respectively. The observed intensity at the detector is a superposition of the two amplitudes and is given by

$$I_{\text{det}} = |U_1 + U_2|^2 = A_1^2 + A_2^2 + 2 A_1 A_2 \cos (\phi_1 - \phi_2), \quad (3a)$$

which can be rewritten as

$$I_{\text{det}} = A^2 \left[1 + \frac{2t a}{a + 2s \tan [\sin^{-1}(\text{NA})]} \cos \left(\frac{4\pi s}{\lambda} \right) + \left(\frac{t a}{a + 2s \tan [\sin^{-1}(\text{NA})]} \right)^2 \right], \quad (3b)$$

where we have assumed that $f_1 = 0$ and $f_2 = 2s(2\pi/\lambda)$, and λ is the wavelength of operation in free space. The simplified loss relation (Equation 2) for the misalignment of two fibers is sufficient for understanding the drop in the output intensity of the sensor as a function of the gap displacement. For a strain sensor, it is useful to plot the detected intensity versus gap-separation s , as shown in Figure 2. We see that the fringe contrast drops as the displacement increases; this is to be expected since the relative intensity of the sensing reflection starts dropping with respect to the reference reflection.

The principle of operation of a quadrature phase-shifted, dual-mode interferometric sensor has been described in detail [7]. Figure 3 shows a typical sinusoidal variation of the output intensity with respect to changes in the phase difference between the reference and the sensing reflections. If the phase difference ϕ varies sinusoidally with time and the peak-to-peak variation is large enough to push the sensor out of its linear range, we observe fringes at the output of the detector as shown in the figure. The basic principle of

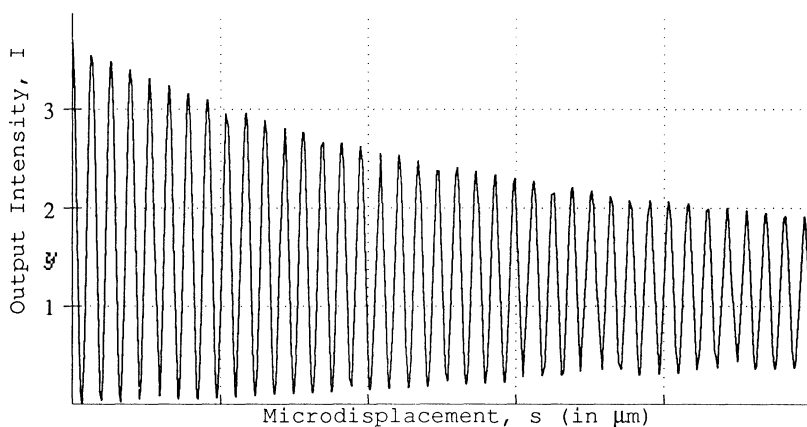


Fig. 2. Therotical output vs. gap separation.

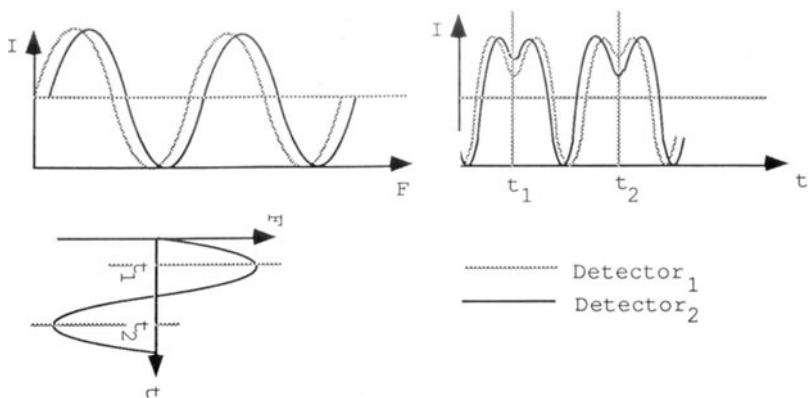


Fig. 3. Phase and time vs. intensity of a Fabry-Perot sensor output.

operation of the detection scheme for a dynamic strain measurement system can now be described by considering two sinusoidal transfer functions out of phase by 90° . Assuming that the transfer function for the first detector (D_1) leads that of the second (D_2), we find that the output waveform for D_1 leads that of D_2 until time t_1 . At time t_1 , the phase f changes direction (because of a change in direction of the strain), and the output waveforms switch their lead-lag properties. We see that the output from D_2 now leads that of D_1 until time t_2 when the strain changes direction again. Keeping track of the lead-lag phenomenon between the two detectors gives us unambiguous information about the relative direction of the strain.

If we had used only one detector, the switch in direction would not be noticeable when the strain changed direction at a peak of the transfer function curve. If the direction change occurs at one peak (of either D_1 or D_2), the other transfer function curve will provide information about the direction change since we now have two signals out of phase by 90° .

Practical methods of obtaining two signals 90° out of phase with respect to one another are shown in Figures 4 (a) and (b). In Figure 4 (a), two single-mode fibers are inserted into one hollow silica tube, and the gap-separations for the two fibers are adjusted actively by moving the fibers in and out of the tube until a 90° phase shift is achieved at the output. Note that two different sources are used in order to avoid interference effects between the two signals returning to the coupler. It may, however, be possible to use a single source and two different lengths of lead fibers for the two sensors such that the difference in the lengths is greater than the coherence length of the laser. Figure 5 (b) is a slight variation of the earlier scheme; here, we use two

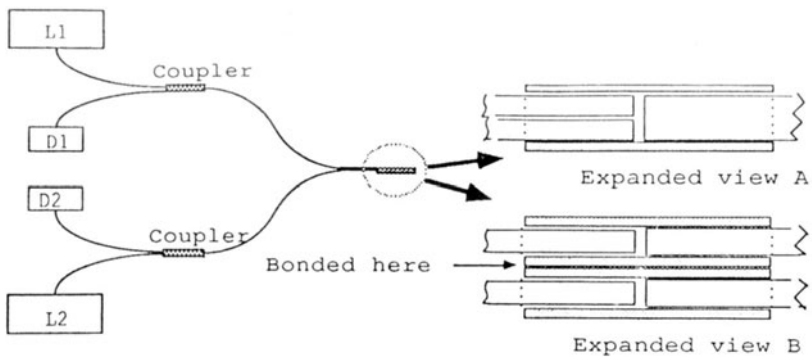


Figure 4. Quadrature phase shifted sensors.

different silica tubes and, once again, adjust the quadrature phase-shift actively. Since the two tubes have external diameters on the order of a few hundred micrometers, the two sensors monitor almost the same environmental perturbations.

To test the validity of the quadrature phase-shifted sensors at high temperatures, the sensor was attached (using the scheme shown in Figure 4b) to a piece of ceramic material using Cotronics 989 adhesive. A typical oscilloscope trace is shown in Figure 5. The figure clearly shows the shift in the lead/lag properties of the two signals as the relative direction of the thermal strain changes from increasing to decreasing as the temperature changes from 500 to 450°C.

RESULTS OF ON-SITE TESTING

For on-site testing several quadrature phase shifted Fabry-Perot sensors were attached, again using the Cotronics 989 adhesive. At the beginning of the tests the filter was

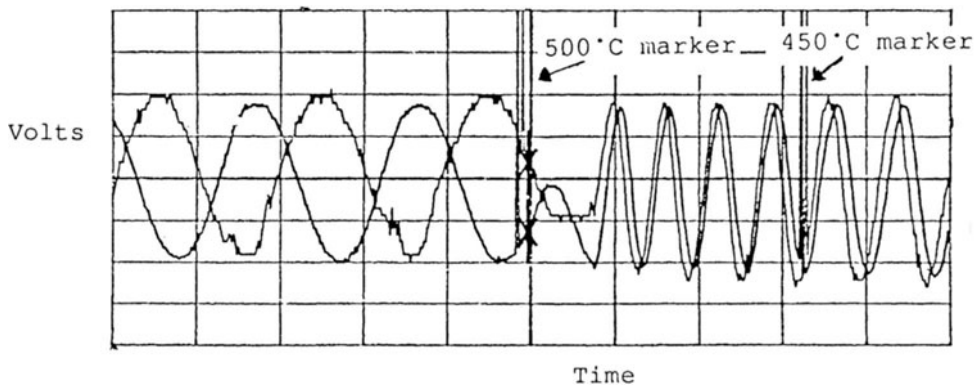


Figure 5. Expanded traces at the point where the kiln went from increasing temperature to decreasing temperature at 500° Celsius.

still warm (100° F) from the heating process it underwent the previous night. The filter vessel was pressurized to 30 psi to check for leaks. During the pressurization the sensors were monitored. The sensor outputs were recorded when pressurization began. An oscilloscope ground trace was started (to provide marks in the trace) when the vessel reached 30 psi. The signal recorded corresponds to a strain of 7.3 μ strain for the induced differential pressure of 30 psi. Figure 6 is a plot of the strain sensor output and a conventional thermocouple vs. time during the test. First electric heaters were used to provide a slow warming of the filter, normally done to prevent thermal shock to the filter. The seven test stages are noted in Figure 6 as: 1) electric heater warm-up, 2) cool-air to the back plate to start torch, 3) cool air increase, 4) flame on, 5) flame out, 6) flame on again and 7) closed bypass valve to induce rapid heating. At 420° C the torch was tuned off and the filter vessel was allowed to cool.

CONCLUSION

In conclusion, we have demonstrated the operation of a quadrature phase-shifted, low-finesse, extrinsic FP sensor and its use in obtaining dynamically varying information by operating it in a quadrature phase-shifted mode. Limitations on the frequency range of operation will be set by the signal processing electronics at the output end. The signal-to-noise ratio (SNR) of the sensor decreases if a large air gap is introduced due to a decrease in fringe contrast. Hence, this sensor will be useful for applications where maximum displacements to be measured are on the order of a few hundred micrometers. Strain sensitivities of 5.54° phase shift / μ strain - cm were obtained.

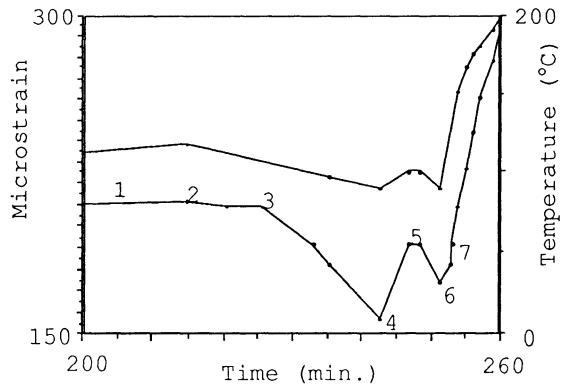


Figure 6. Strain and temperature vs. time for a Fabry-Perot sensor during heat-up.

The sensor was successfully demonstrated as a thermally induced strain monitor in an industrial environment up to 450° C (the limitation of the fiber coating not the sensor itself). The sensor has been used successfully tested in a laboratory environment up to 975° C with no fiber coating.

ACKNOWLEDGMENTS

Research on this project was sponsored by the United States Department of Energy, Morgantown Energy Technology Center, under contract number DE-AC21-89MC25159.

REFERENCES

1. T. Yoshino, K. Kurosawa, K. Itoh, and T. Ose, IEEE J. Quantum Electron. QE-18, 1624 (1982).
2. K. L. Belsley, J. B. Carroll, L. A. Hess, D. R. Huber, and D. Schmadel, Proc. Soc. Photo-Opt. Instrum. Eng. 566, 257 (1985).
3. A. D. Kersey, D. A. Jackson, and M. Corke, Opt. Comm. 45, 71 (1983).
4. C. E. Lee and H. F. Taylor, Electron. Lett. 24, 193 (1988).
5. J. Putz, J. Putz, A. Wicks, and T. Diller, "Thin-film shear stress gage", Proc. ASME Winter Annual Meeting, Symposium on Micro Structures, Sensors and Actuators, Dallas. (1990).
6. K. A. Murphy, M. S. Miller, A. M. Vengsarkar, and R. O. Claus, "Elliptical core, two-mode, optical fiber sensor implementation methods", To be published J. Lightwave Technol. (1991).
7. K. A. Murphy, M. F. Gunther, A. M. Vengsarkar, and R. O. Claus, "Quadrature phase shifted extrinsic Fabry-Perot fiber optic sensors," Opt. Lett., Vol. 16, p. 273, 1991.